International Journal of Civil Engineering

Hydraulic Structure Engineering

Technical Note

Numerical simulation of the interaction of a broken wave and a vertical breakwater

F. Hajivalie[1], A. Yeganeh Bakhtiary[2,*]

Received: July 2009, Revised: August 2010, Accepted: September 2010

Abstract

In this paper, a two-dimensional Reynolds Averaged Navier-Stokes (RANS) model is developed to simulate the shoaling, breaking and overtopping of a solitary wave over a vertical breakwater. Turbulence intensity is described by using a k-ε turbulence closure model and the free surface configuration is tracked by Volume Of Fluid (VOF) technique. To validate the numerical model the simulation results is compared with the Xie (1981) experimental data and a very good agreement between them is observed. The results revealed that wave height and wave energy decrease considerably during the reflection from vertical wall, which illustrates a considerable energy lost during the impaction and wave overtopping process. The turbulence production during the broken wave interaction with vertical breakwater is very significant; consequently the vertical breakwater undergoes sever turbulent and dynamic drag force.

Keywords: RANS model, shoaling, wave breaking, wave overtopping, k-ε turbulence closure model, VOF technique, solitary wave.

1. Introduction

Wave breaking in the nearshore zone forms a huge turbulent bore propagating towards the coastal breakwaters and such violent flow may cause different types of breakwater failure. Vertical breakwaters are preferred to rubble-mound breakwaters because the vertical breakwaters are more economic and take less time to construct. The vertical breakwater acts as a rigid structure and transmits most of the impinged broken wave forces to its foundation: it makes a vertical breakwater to become so sensitive to its foundation damages. Therefore, it is very important to study the broken wave interaction with a vertical breakwater. Most of the existing studies have been restricted to the interaction of nonbreaking waves with the vertical breakwater.

Xie [1] experimentally studied the interaction of standing wave with a vertical breakwater and measured the distributions of maximum horizontal orbital velocities at the wave node and antinode. Later on Gao and Inouchi [2] investigated experimentally the broken wave impacts on a vertical breakwater placed over a sloping bed. They pointed out that when the incident wave breaks, the broken wave climbed up the face of breakwater and then fallen back; whereas little information about wave movement during the process of breaking, impaction and reflection is presented. Sakakiyama and Liu [3] experimentally studied the free surface displacements and velocity field in front of a caisson breakwater with wave-dissipating blocks, together with both nonbreaking and breaking wave acting on a caisson breakwater. They studied the generation of turbulence by wave-breaking and by the flow through the porous armor layer.

The complexity involved in the wave interaction with vertical breakwaters has directed researchers to use the numerical simulation. Suh et al. [8] used a numerical model to compute the reflection of regular and irregular waves from a partially perforated-wall caisson breakwater. Gislason et al. [10] studied the hydrodynamics of 2D laminar flow condition in front of a vertical breakwater. Hajivalie and Yeganeh-Bakhtiary [4] developed a numerical model based on Reynolds Averaged Navier Stokes (RANS) equations with a *k-ε* turbulence closuring model, to study the breakwater steepness effects on the standing waves formation. The free surface configuration was tracked by Volume Of Fluid (VOF) technique suggested by Hirt and Nichols [5]. Yeganeh-Bakhtiary et al. [6], employed this model to simulate the interaction process of the wave overtopping with a vertical breakwater.

On the other hand, solitary waves were usually utilized to

* *Corresponding Author:Yeganeh@iust.ac.ir*
1 PhD Candidate, School of Civil Engineering, Iran University of Science and Technology Narmak, Tehran 16844, IRAN
2 Assistant Professor, Enviro-Hydroinformatics COE, School of Civil Engineering, Iran University of Science and Technology Narmak, Tehran 16844, IRAN

study the behavior of a broken wave approaching a shore. For example Grilli et al. [7] numerically studied wave breakings process on different slopes by simulating the shoaling and breaking of solitary waves on slopes from 1:100 to 1:8 using a fully nonlinear wave model based on potential flow equations. The wave characteristics at and beyond the breaking point is studied and a breaking criterion based on the nondimensional slope parameter is derived. Chang et al. [8] experimentally studied the run up flow and related pressure of solitary waves on a 1:20 beach; they measured swash flow velocity and compared it with the existing analytical solution. They observed extra pressure exerted by the impact of swash flow. Lin and Karunarathna [9], Ryu et al. [10] and Hsiao and Lin [11] studied the interaction of solitary waves with different type of breakwaters and seawall.

Although there were several experimental and numerical studies about the interaction of nonbreaking wave and vertical breakwaters and also about breaking and overtopping of solitary waves over coastal structures, there has been little study about the interaction of a broken wave with a vertical breakwater. Thus, in this study, we investigated numerically the ensuing hydrodynamic processes involved in the interaction effect of a broken wave with a vertical breakwater. For this purpose, an extended version of the pervious model of Hajivalie et al. [4] with introducing the initial and boundary conditions corresponding to broken wave in front of vertical breakwaters were employed. Finite difference solutions to the governing equations were obtained, while the free surface is tracked by using the VOF technique. Below, Section 2 gave the mathematical framework for the model while Section 3 discusses the numerical model. In Section 4, the numerical results were presented and conclusions were drawn in Section 5.

2. Mathematical Formulation

In this section, the equations governing the flow and turbulence fields are presented. Thereafter, the initial and boundary conditions were discussed. The RANS equations, which describe the mean flow field, in closure with a k-ε turbulence model are applied to simulate the turbulent flow in front of a vertical breakwater.

2.1. Governing equations

The governing equations consisted of the continuity, momentum and the k-ε equations were introduced in two-dimensional coordinates as follow:

$$\frac{\partial U}{\partial x}+\frac{\partial W}{\partial z}=0 \tag{1}$$

$$\frac{\partial U}{\partial t}+U\frac{\partial U}{\partial x}+W\frac{\partial U}{\partial z}=-\frac{1}{\rho}\frac{\partial P}{\partial x}+\frac{\partial}{\partial x}\left(2\Gamma\frac{\partial U}{\partial x}\right)+\frac{\partial}{\partial z}\left(\Gamma\left(\frac{\partial U}{\partial z}+\frac{\partial W}{\partial x}\right)\right) \tag{2}$$

$$\frac{\partial W}{\partial t}+U\frac{\partial W}{\partial x}+W\frac{\partial W}{\partial z}=-\frac{1}{\rho}\frac{\partial P}{\partial z}-g+\frac{\partial}{\partial x}\left\{\Gamma\left(\frac{\partial U}{\partial z}+\frac{\partial W}{\partial x}\right)\right\}+\frac{\partial}{\partial z}\left(2\Gamma\frac{\partial W}{\partial z}\right) \tag{3}$$

$$\frac{\partial k}{\partial t}+U\frac{\partial k}{\partial x}+W\frac{\partial k}{\partial z}=\frac{\partial}{\partial x}\left[\left(\nu+\frac{\nu_t}{\sigma_k}\right)\frac{\partial k}{\partial x}\right]+\frac{\partial}{\partial z}\left[\left(\nu+\frac{\nu_t}{\sigma_k}\right)\frac{\partial k}{\partial z}\right]+p_r-\varepsilon \tag{4}$$

$$\frac{\partial \varepsilon}{\partial t}+U\frac{\partial \varepsilon}{\partial x}+W\frac{\partial \varepsilon}{\partial z}=\frac{\partial}{\partial x}\left[\left(\nu+\frac{\nu_t}{\sigma_\varepsilon}\right)\frac{\partial \varepsilon}{\partial x}\right]+\frac{\partial}{\partial z}\left[\left(\nu+\frac{\nu_t}{\sigma_\varepsilon}\right)\frac{\partial \varepsilon}{\partial z}\right]+C_{1\varepsilon}\frac{\varepsilon}{k}P_r-C_{2\varepsilon}\frac{\varepsilon^2}{k} \tag{5}$$

$$p_r=\nu_t\left[2\left\{\left(\frac{\partial U}{\partial x}\right)^2+\left(\frac{\partial W}{\partial z}\right)^2\right\}+\left(\frac{\partial U}{\partial z}+\frac{\partial W}{\partial x}\right)^2\right] \tag{6}$$

$$\nu_t=C_\mu\frac{k^2}{\varepsilon},\qquad \Gamma=\nu+\nu_t \tag{7}$$

where U and W are the mean velocity components of flow in x (stream-wise) and z (vertical) direction, respectively; P is the mean pressure; g is the acceleration of gravity; ρ is the fluid density; ν and ν_t are respectively the kinematic and kinetic eddy viscosity; k is the turbulence kinetic energy; p_r is the production of turbulence kinetic energy; ε is the turbulence dissipation rate. The model constants were set according to Launder and Spalding [12] presented in Table 1.

2.2. Initial and Boundary Condition

The initial flow motion was specified with the zero mean velocities and hydrostatic pressure. The initial conditions of the turbulence field were set according to Lin [13] as follows:

$$k=\frac{1}{2}u_t^2\ ,\ u_t=\delta c_i\ ,\ \delta=0.0025 \tag{8}$$

$$\varepsilon=C_\mu\frac{k^2}{\nu_t}\ ,\ \nu_t=\zeta\nu\ ,\ \zeta=0.1,\ C_\mu=0.09 \tag{9}$$

where ci is the wave celerity at the inlet boundary, C_μ is the empirical coefficient suggested by Rodi [14], δ and ζ are the model's constants.

Boundary conditions at the free surface, bottom, inlet and outlet were defined in the following. The free surface motion was tracked by the VOF technique [5], which satisfies both the kinematic and dynamic free surface conditions, the conservation of F or the volume fraction of fluid with the donor-acceptor algorithm and was expressed as follows:

$$\frac{\partial F}{\partial t}+U\frac{\partial F}{\partial x}+W\frac{\partial F}{\partial z}=0 \tag{10}$$

The flow turbulence was not spread to free surface and therefore the vertical flux of k and ε on the free surface should reach to zero:

$$\frac{\partial k}{\partial n}=0\quad ,\quad \frac{\partial \varepsilon}{\partial n}=0 \tag{11}$$

here n is the normal vector. At the bottom, the wall function was used to account for the rough bed condition. Based on the numerical analysis, the gradient of the averaged velocity was expressed as follows:

$$\frac{\partial U}{\partial z}=\frac{u_*}{\kappa z} \tag{12}$$

Table 4. The constants in k-ε turbulence model [12]

C_μ	$C_{1\varepsilon}$	$C_{2\varepsilon}$	σ_k	σ_ε
0.09	1.44	1.92	1.0	1.3

here z is the distance from the bed, u_* is the shear velocity ($=\sqrt{\tau_w/\rho}$), τ_w is the shear stress in the flow direction and κ is the von-Karman constant (=0.41). If the above equation is integrated, the logarithmic velocity distribution at the boundary layer is obtained:

$$\frac{U}{u_*}=\frac{1}{\kappa}\ln\left(E\frac{u_* z}{\nu}\right) \tag{13}$$

where E is a constant value ($\approx$9.0, [14]). Using the final value of shear velocity, u_* the boundary values of k and ε at the bed can be defined as

$$\varepsilon=\frac{u^3{}_*}{\kappa y\left[1-\exp\left(-\frac{u_* z}{26\nu_t}\right)\right]} \tag{14}$$

$$\nu_t=\kappa u_* y\left[1-\exp\left(-\frac{u_* z}{26\nu}\right)\right] \tag{15}$$

$$k=\frac{u_*^2}{\sqrt{C_d}} \tag{16}$$

In calculating the rate of turbulence dissipation a descending function was used. Implementing this function lead to a nearly exact value of for the low turbulence condition, which is acceptable in case of the laminar sub-layer, while the turbulence production and its dissipation is only due to the bed friction. At the inlet and outlet boundaries Neumann continuative boundary condition were assumed.

$$\begin{aligned} &k_{1,j}=k_{2,j}\quad,\quad k_{i_{\max-1},j}=k_{i_{\max-2},j}\\ &\varepsilon_{1,j}=\varepsilon_{2,j}\quad,\quad \varepsilon_{i_{\max-1},j}=\varepsilon_{i_{\max-2},j}\end{aligned} \tag{17}$$

At the inlet boundary, the generating-absorbing boundary condition, introduced by Petit et al. [16] was implemented. By imposing this condition, the incident waves can be generated while the reflected waves from the vertical breakwater were absorbed simultaneously. This prohibits the collision (intermixing) of the generated and reflected waves that propagated in opposite direction of the interested zone:

$$\frac{\partial R_r}{\partial t}+C_r\frac{\partial R_r}{\partial x}=0 \tag{18}$$

$$R_r=R_t-R_{in} \tag{19}$$

where C_r is the celerity of reflected wave, R_r, R_t and R_{in} are the variable associated with the reflected, computed and the theoretical wave values represents velocity, pressure, and free surface displacement and R_{in} is the calculated by the Airy or Stokes second order theory.

The outlet consisted of two different kinds of boundaries: (i) for solid boundary of vertical breakwater, turbulence boundary condition was defined; and (ii) over the breakwater, open boundary condition was defined to allow wave overtopping as follows:

$$\frac{\partial u}{\partial t}+c\frac{\partial u}{\partial x}=q_o \tag{20}$$

here q_o is the overtopping discharge, computed with Franco and Franco) [17] overtopping formula:

$$q_o=\sqrt{gH_s{}^3}\times\left(0.082\exp\left(\frac{-3R_c}{H_s}.\frac{1}{\gamma_\beta\gamma_s}\right)\right) \tag{21}$$

where H_s is the significant incident wave height, γ_β is the factor of incident wave angel (=1.0), γ_s is the factor of permeability (=1.0) and R_c is the breakwater freeboard.

3. Numerical Model

The governing equations were the two-dimensional momentum and continuity, volume of fluid change function and k-ε equations. The governing equations were discretized in an Eulerian staggered grid with rectangular cells. Scalar variables such as pressure and density were calculated from the ordinary nodes and the velocity components were calculated from the staggered grid around the cells. Thus, the discretized continuity equation was converted to a pressure correction equation that was defined on the scalar control volumes. Figure 1 illustrated the staggered grid presented in the x-y plane of the Cartesian coordinate system. The two-dimensional equations were discretized by finite-difference methods. In summary, the calculation procedure was as follows:

- Using the momentum equations and the respective values of time step n, the velocity components of time step $n+1$ were approximated.
- Since the velocity obtained by the momentum equations might not satisfy the continuity equation, the pressure in every cell should change so that the new velocities calculated from the pressure variations satisfy the continuity equation. This was done by iteration.
- Using the k-ε equations, their values were calculated. Then, implementing the new values, the turbulent viscosity was calculated and used in the next step.
- The value of the function F for each cell was defined at time step $n+1$. Therefore the new position of the fluid was defined.
- (5) After calculating the time step size, d_t, the next step of calculations was performed at time $t+d_t$,

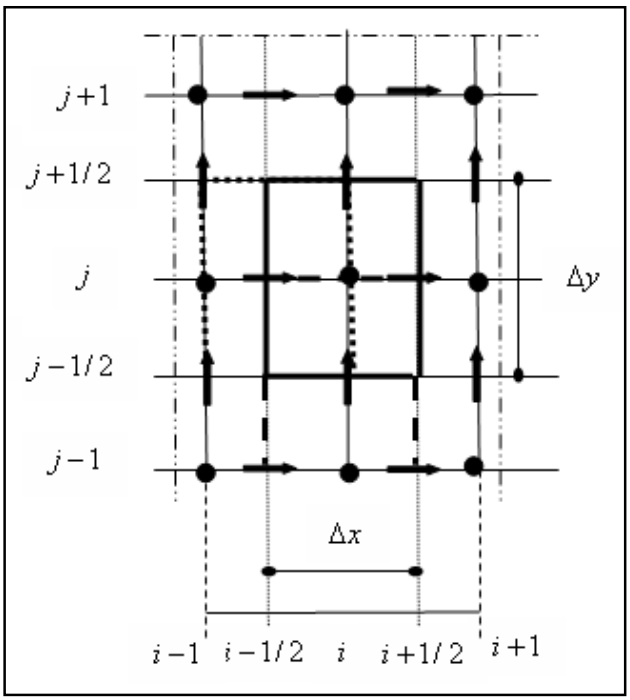

fig. 1. Grid geometry, control volumes of scalar and vector quantities and location of variables in the x-y plane

3.1. Stability of the numerical scheme

Stability should be controlled mainly by the value of d_t: its value was consider in the following [15]:

•The fluid was not allowed to travel more than one computational cell in each time step:

$$\Delta t \le Min\left(\frac{\Delta x}{|U_x|}, \frac{\Delta y}{|U_y|}\right) \tag{24}$$

•Surface waves was not allowed to travel more than one cell in each time step:

$$\Delta t \le Min\left(\frac{\Delta x}{\sqrt{g h_{\max}}}\right) \tag{25}$$

where h_{max} is the maximum depth of flow.

•The relative variation of k and in a time step should be significantly less than unity:

$$\Delta t \le Min\left(\frac{k}{\varepsilon}\right) \tag{26}$$

$$\Delta t \le Min\left(\frac{1}{C_{2\varepsilon}}\frac{k}{\varepsilon}\right) \tag{27}$$

•The size of time step was adjusted to satisfy the diffusion stability condition:

$$\Delta t \le Min\left(\frac{\Delta x^2 \Delta y^2}{2\nu_e\left(\Delta x^2 + \Delta y^2\right)}\right) \tag{28}$$

here $\nu_e = \nu + \nu_t$

4. Results and Discussion

4.1. Model validation

To assess the accuracy of the numerical model we should compare the numerical result with experimental data of interaction between waves and vertical breakwater. As it was mentioned before to the best knowledge of the authors there is no experimental data available on the study of interaction of breaking and/or broken waves and vertical breakwater, therefore Xie's [1] experimental data for nonbreaking wave has been employed. In the experiments, nonbreaking waves were used to develop standing waves in front of a vertical breakwater. Fig. 2 depicts the experimental set up of vertical breakwater by Xie [1]. The experiment was conducted in a 38 m long, 0.8 m wide and 0.6 m deep wave flume. The water depth was equal to 0.45 m in the beginning of the flume and reached to 0.3 at the flat bed near the breakwater with a 1:30 slope.

Three different tests of Xie [1] experiments were simulated and the characteristics of these tests was summarizes in Table 2. In the numerical simulations, the computational domain has total length of 14.5 m and a height of 0.7 m, the length of computational domain is shortened than the experimental flume to reduce the computation times (see Fig. 3). At the inlet boundary, Airy waves theory was employed to generate the incident waves into computational domain (see Chapter 2.2). Incident waves started to propagate into the numerical domain at beginning of the simulation. The interferences of incident waves impinged on a vertical breakwater and the reflected

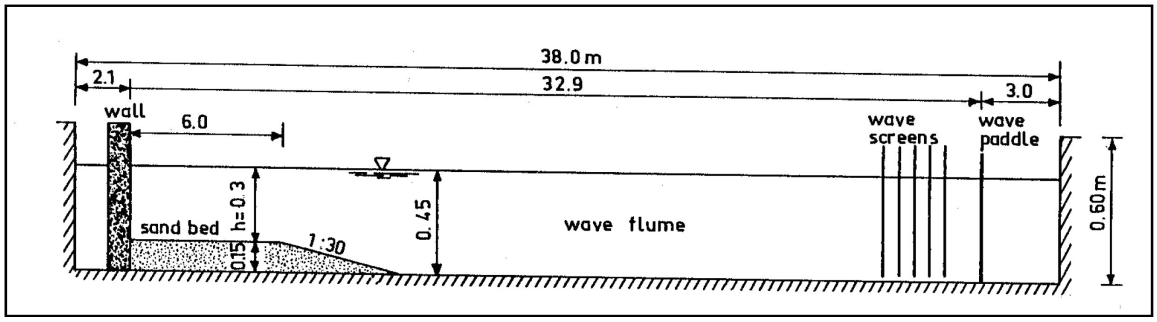

Fig. 2. The sketch of physical model [1]

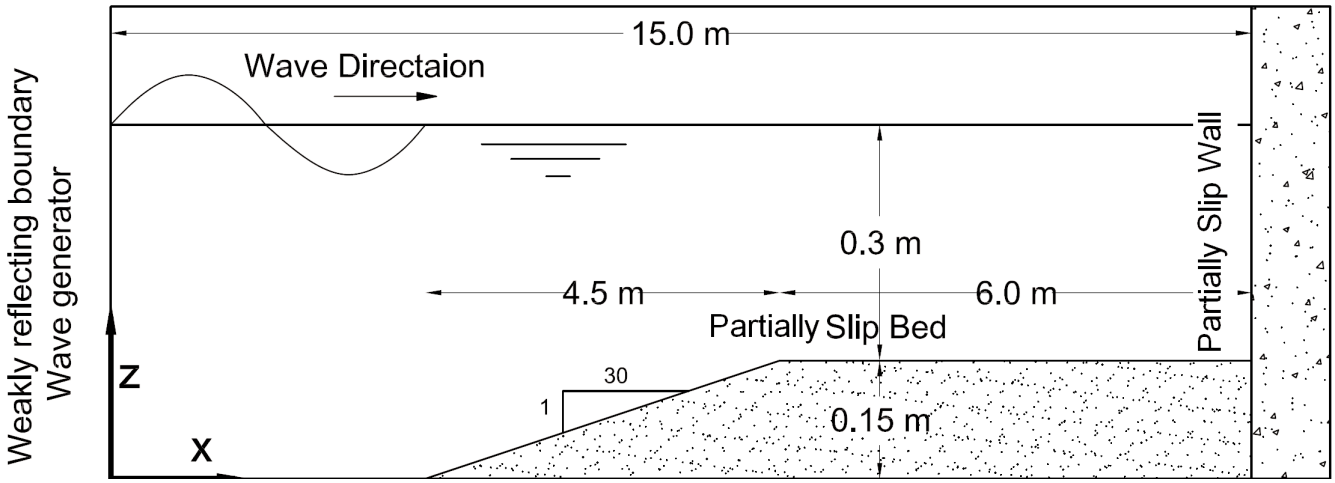

Fig. 3. Sketch of numerical domain

Table 4. The constants in k-ε turbulence model [12]

The incident wave characteristics	H(m)	T(s)	d(m)	L(m)	Duration of numerical simulation (s)
Test No. 1	0.05	2.41	0.45-0.3	4.00	24.1
Test No. 2	0.065	1.53	0.45-0.3	2.40	15.3
Test No. 3	0.06	1.86	0.45-0.3	6.00	18.6

waves from it produce the standing waves in front of vertical breakwater. The flow velocities at nodes and antinodes then can be observed and compared with that of the experimental one. Xie [1] measured maximum horizontal velocity in two sections, near the first node of standing waves and halfway of node and antinode; the same velocities computed by numerical model were compared with the experiments in Fig. 4. As seen from the figure there is a very good agreement between the numerical results and experimental data. The figure also indicated that the difference between the numerical results and experimental data increase with the increasing of H/d.

To best knowledge of the authors, the measuring turbulence parameters for broken waves in front of vertical breakwater has not been available yet. It is ineluctably used one of the cases of the Hsiao and Lin [11] experimental data to validate the turbulence field of the model. Hsiao and Lin [11] experiments were carried out in a wave flume, 22 X 0.5 X 0:75 m. Solitary wave broken on a 1:20 sloping beach with 3.6 m length, the incident wave height and water depth were 0.07 m and 0.2 m, respectively. Fig. 5 shows both the result of the simulation model on the turbulence energy and that presented by Hsiao and Lin [11] at the breaking point. The solitary wave was breaking as a plunging breaker with generating a considerable turbulent energy at almost the same point. The maximum turbulent energy generated from the simulation model was at the approximately same order of experiments and the trend of the generated turbulent kinetic energy is very similar in both cases. The figure indicates that the model describes the turbulence generation with a very satisfactory accuracy.

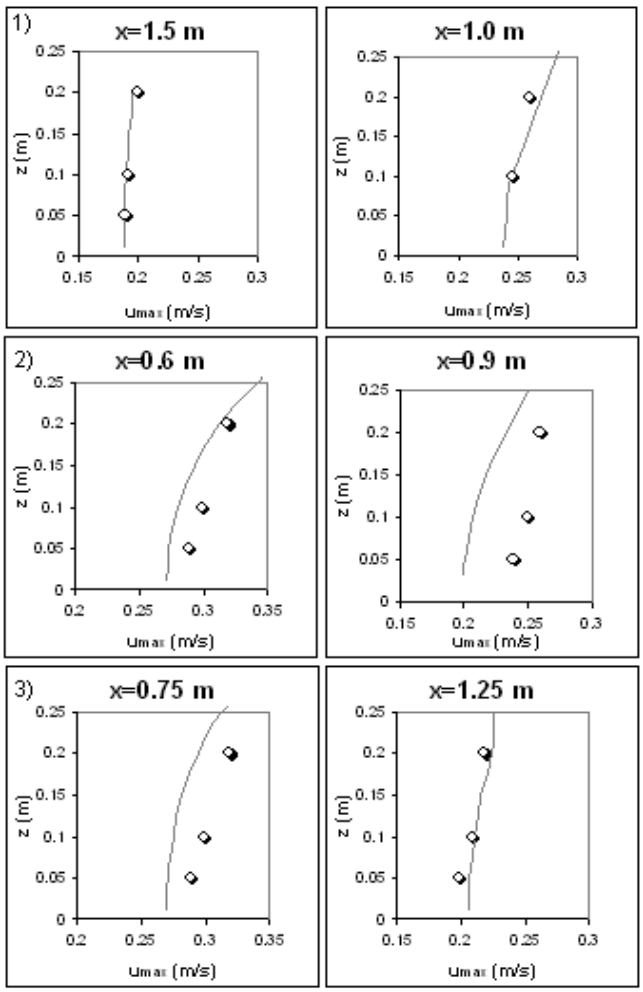

Fig. 4. Comparison of numerical model results and Xie's experimental data, tests No. (1,2,3), continues line: numerical results, circles: Xie [1] experimental data

4.2. Wave field and transformation

To simulate the interaction of a broken wave and a vertical breakwater the previous numerical domain has been employed. To simulate the broken wave, a 0.21 m height solitary wave with the wave celerity of 2.67 m/s was generated in the numerical domain. The vertical breakwater was 0.65 m high and 1.0 m wide. Fig. 6 shows the free surface configuration during the numerical simulation. At the beginning the solitary wave

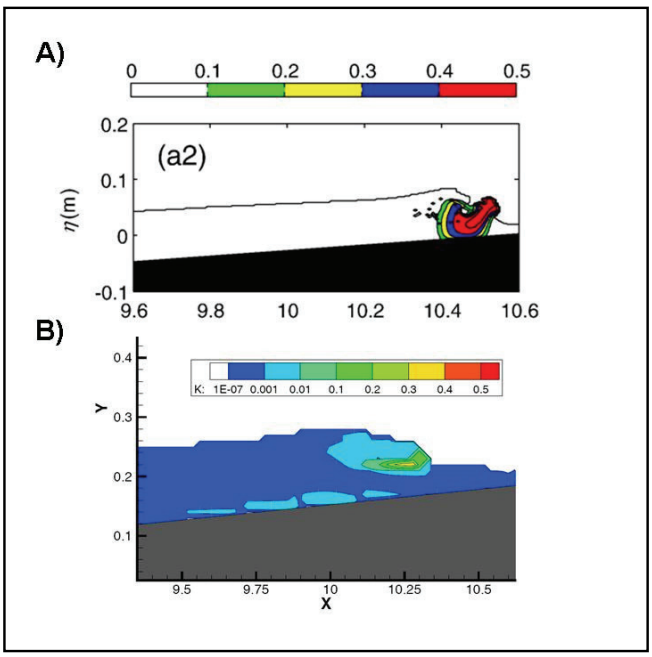

Fig. 5. Distribution of turbulent energy at breaking point; A) experimental data of Hsiao and Lin [11] and B) the simulation result

progressed into the numerical domain. As it reach over the slope, due the shoaling effect the wave height started to increase till it reached to a breaking height equal to 0.24 m (which fulfill the McCowan breaking criteria), at this stage a plunging breaker was observed and the broken wave impact to the vertical breakwater. A portion of flow body overtopped on the vertical breakwater and the rest of flow body reflected from the breakwater. The maximum observed overtopping discharge was about 0.14 (m^3/s) per length unit. The reflected wave height was 0.15 m, about 70% of the initial wave height that demonstrates noticeable energy dissipation during the breaking and overtopping process.

Fig. 7 shows the variation of horizontal and vertical velocities. Fig.7-a indicated that wave crest has the maximum horizontal velocity, which increase with increasing of wave height during the shoaling effect. It was also indicated that the impinging velocity - with maximum of 1.0 m/s- was larger than reflecting velocity -with maximum of 0.5 m/s, which shows that the energy lost happened during the wave impinging and overtopping the vertical breakwater.. Fig. 7-b shows that at the front of progressive wave, the vertical velocity was upward at the front of the vertical wall and it was downward at the back side of wave crest. It was also indicated that the vertical velocity increased during the shoaling effect and it was noticeably decreased in the reflected wave.

The particle velocity of broken wave near the breakwater at impact and reflection stages from the vertical breakwater is shown in Fig. 8. The figure indicated that during the wave overtopping stage, a strong jet flow transfer over the crown of vertical breakwater, namely the jet velocity was more than 2 m/s in some instance. At this condition, the vertical breakwater experienced a huge dynamic drag force. Whereas, Fig. 8-b indicated that the breakwater foundation faced a high speed undertow flow during the reflection stage, which may influence the breakwater stability.

4.3. Turbulence Field

Fig. 9 shows the quantity of k and ε during the numerical simulation. As seen from the figure, before the broken wave reached to the bed slope, the maximum amount of k and ε were observed near the bottom boundary layer. However, during in the broken wave transform over sloped bed, the amount of turbulence kinetic energy increases significantly in the vicinity of free surface. On the other hand as the wave height started to increase due the shoaling effect, turbulence energy and its dissipation rate increased at the wave surface, while it reached to its maximum at the breaking point. when the broken wave impacted to the vertical breakwater, due the huge change in velocity orientation and quantity because of wave reflection and overtopping, the turbulence intensity increased at the vicinity of the breakwater, consequently the breakwater crown experiences a violent turbulent condition when the jet flow overtopped the breakwater while lee side breakwater wall faced the turbulent produced by wave reflection.

It was also observed that the order of maximum amount of k and ε at the breaking wave surface was about two orders more than the order of the maximum of these parameters at the bottom boundary layer but it was almost the same order as the overtopping jet flow.

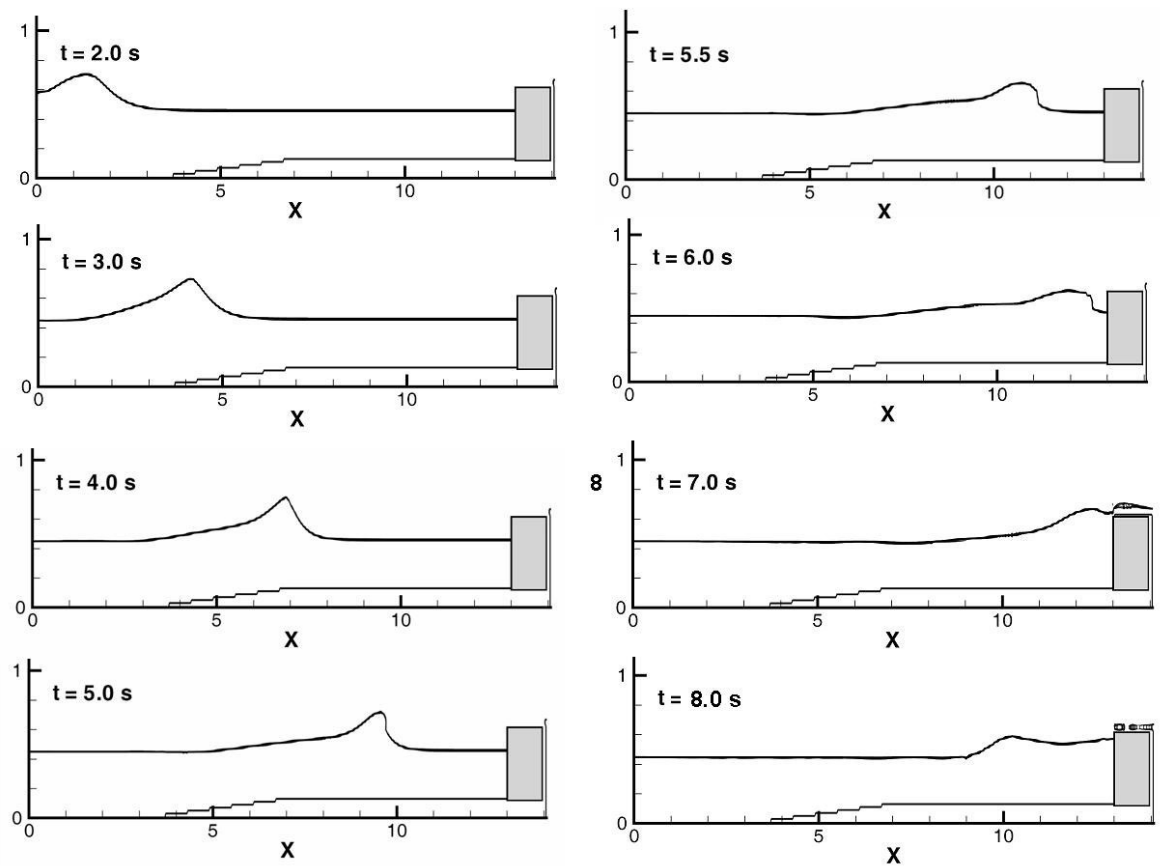

Fig. 6. Snapshots of breaking wave development in front of vertical breakwater

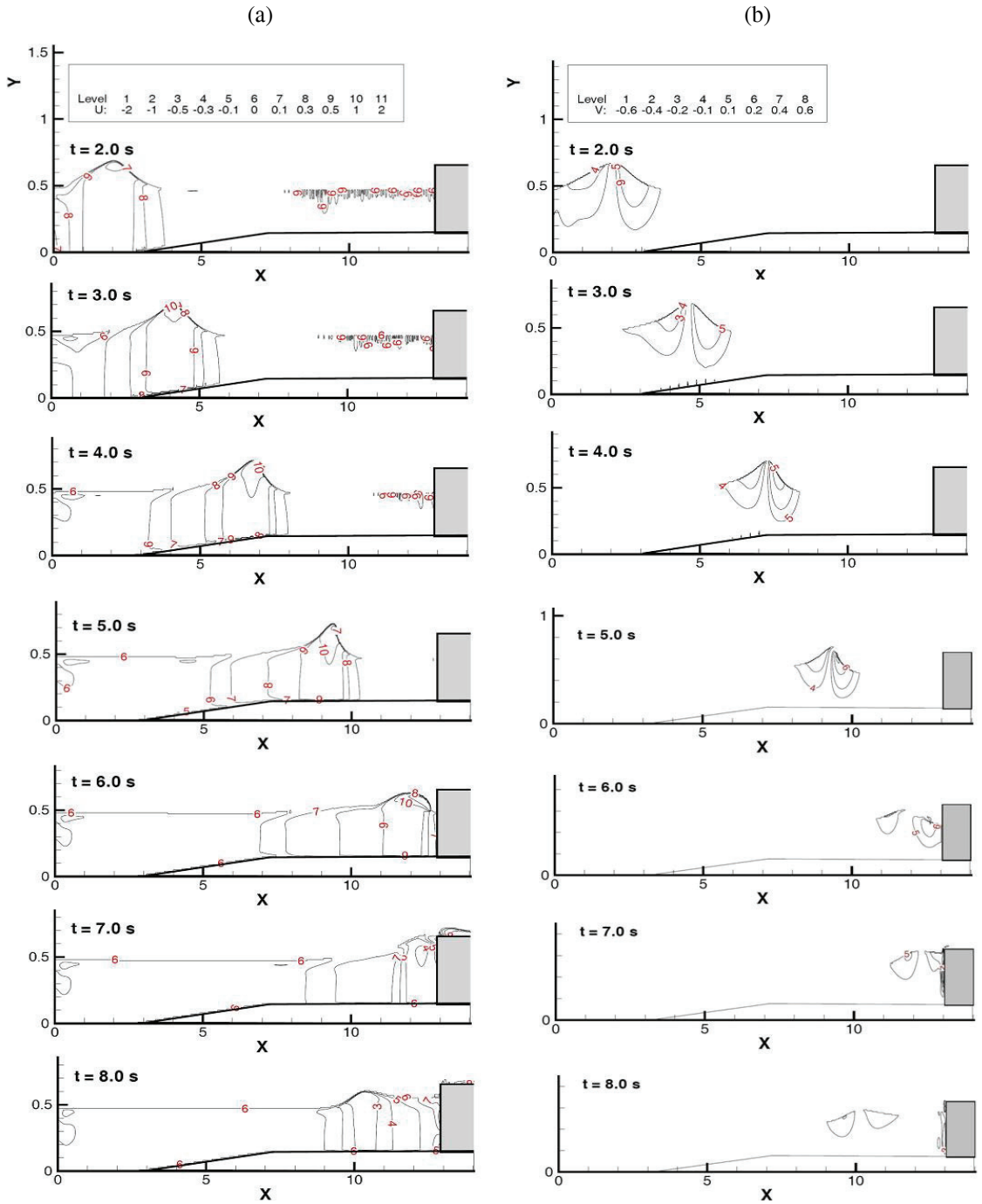

Fig. 7. Variation of a) U and b) V during shoaling, wave breaking and wave overtopping

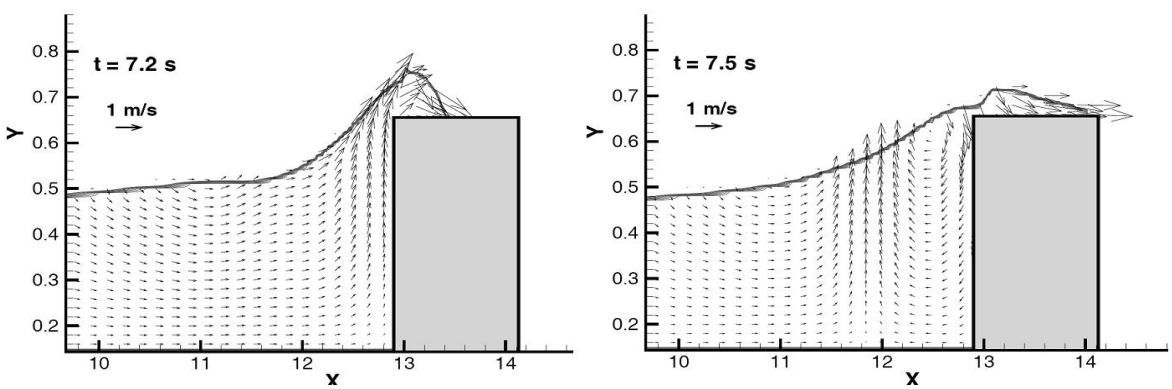

Fig. 8. Snapshots of velocity vectors since wave impaction and overtopping over vertical breakwater

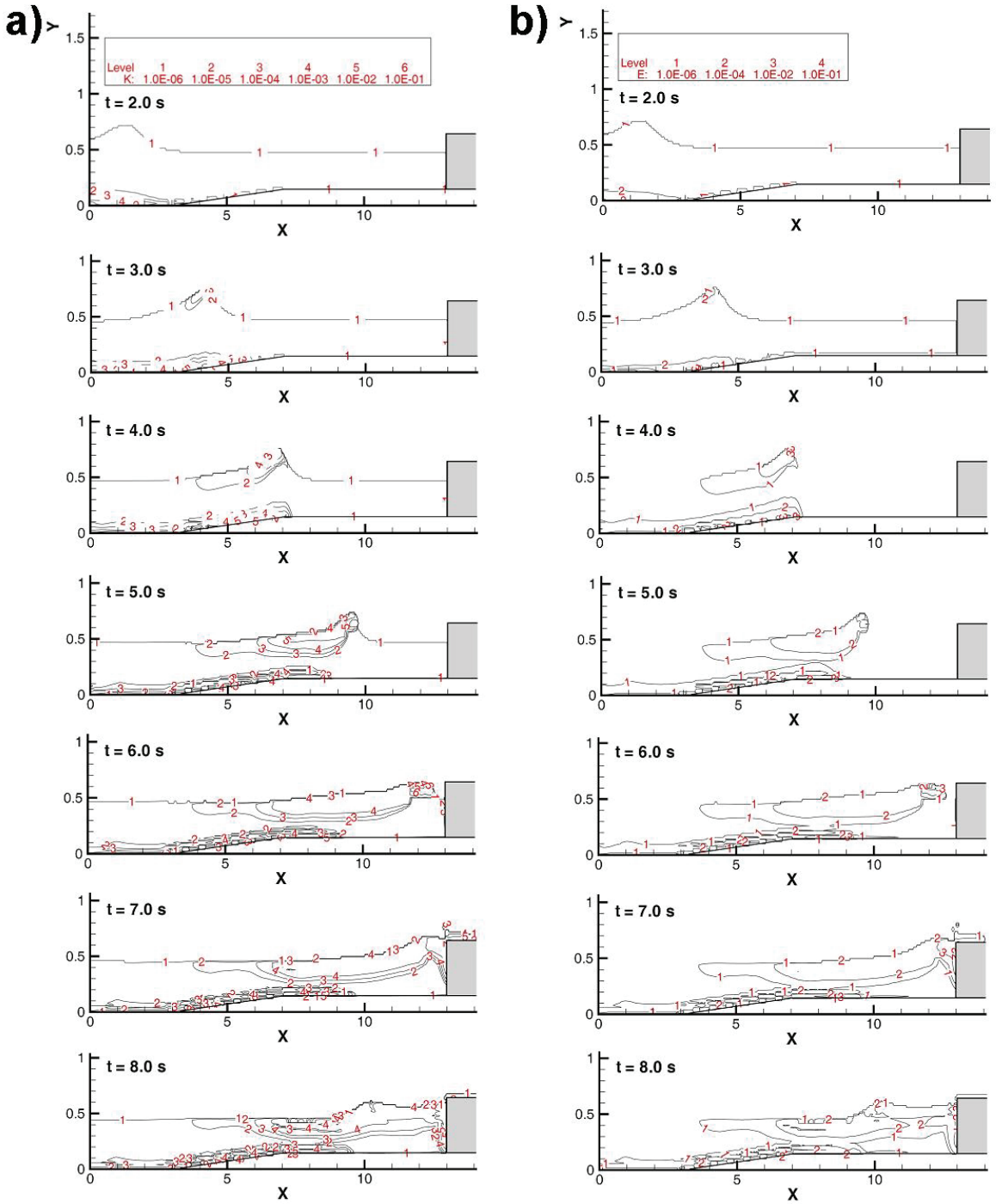

Fig. 9. Variation of a) k and b) ε during shoaling, wave breaking and wave overtopping

5. Conclusion

A 2D numerical model based on RANS equation was been developed to study the interaction between a broken wave with a vertical breakwater. The wave surface configuration was traced by the VOF method and a k-ε model was closured to estimate the turbulence intensity. The model was not validated against the experimental data of broken waves in front of vertical breakwaters because the suitable data set has not been available currently. However, to demonstrate the model capacity the numerical model was validated using the Xie [1] experimental data for nonbreaking wave interaction with vertical breakwater and for the turbulence field, a numerical experiment was performed similar to one of the cases reported by Hsiao and Lin [11]. From this numerical study, the following conclusions were drawn:

- Both wave height and velocity decrease considerably after wave reflection, this indicates that wave energy has been dissipated during the impaction and overtopping process.
- Turbulence intensity at the vicinity of breakwater and in the violent jet flow over the breakwater has the same order as breaking point. It means that the interaction of broken wave and the breakwater has a comparable role in turbulence production with breaking process.
- Breakwater crown experiences significant turbulence condition and dynamic drag forces.

References

[1] Xie S. L. 1981. Scouring pattern in front of vertical breakwaters and their influence on the stability of the foundation of the breakwaters. Delft University of Technology, Delft, pp. 61.

[2] Gao X, Inouchi K. 1998. The characteristics of scouring and deposition in front of vertical breakwaters by broken clapotis. Coastal Engineering Journal 40.

[3] Sakakiyama T, Liu PLF. 2001. Laboratory experiments for wave motions and turbulence flows in front of a breakwater. Coastal Engineering 44:117-139.

[4] Hajivalie F, Yeganeh-Bakhtiary A. 2009. Numerical Study of Breakwater Steepness Effect on the Hydrodynamics of Standing Waves and Steady Streaming. Journal of Coastal Research SI 51:514-518.

[5] Hirt C, Nichols BD. 1981. Volume of fluid (VOF) method for the dynamics of free boundaries. Journal of Computational Physics 39.

[6] Yeganeh-Bakhtiary A, Hajivalie F, Hashemi Javan A. 2010. Steady Streaming and Flow Turbulence in front of Vertical Breakwater with Wave Overtopping. Applied Ocean Research: 32; 91-102.

[7] Grilli ST, Svendsen IA, Subramanya R. 1997. Breaking criterion and characteristics for solitary waves on slopes. Journal of Waterway Port Coastal and Ocean Engineering-Asce 123:102-112.

[8] Chang YH, Hwang KS, Hwung HH. 2009. Large-scale laboratory measurements of solitary wave inundation on a 1:20 slope. Coastal Engineering 56:1022-1034.

[9] Lin P, Karunarathna ASA. 2007. Numerical study of solitary wave interaction with porous breakwaters. Journal of Waterway Port Coastal and Ocean Engineering-Asce 133:352-363.

[10] Ryu YG, Chang KA, Mercier R. 2007. Runup and green water velocities due to breaking wave impinging and overtopping. Experiments in Fluids 43:555-567.

[11] Hsiao SC, Lin TC. 2010. Tsunami-like solitary waves impinging and overtopping an impermeable seawall: Experiment and RANS modeling. Coastal Engineering, 57:1-18.

[12] Launder BE, Spalding DB. 1971. The numerical computation of turbulent flow. Journal of Computational Mechanic in Application of Mechanic and Engineering 3.

[13] Lin P. 1998. Numerical modeling of breaking waves. Cornell University.

[14] Rodi W. 1980. Turbulence model and their application in hydraulic-A state-of-the-art review. IAHR.

[15] Lemos CM. 1992. A simple numerical technique for turbulent flows with free surfaces. International Journal for Numerical Methods in Fluids 15:127-146.

[16] Petit HAH, van Gent MRA, van Den Boscj P. 1994. Numerical simulation and validation of plunging breakers using a 2D Navier- Stokes model. 24th International Conference on Coastal Engineering, Kobe, Japan, pp. 511-524.

[17] Franco C, Franco L. 1999. Overtopping formulas for caisson breakwaters with nonbreaking 3D waves. Journal of Waterway Port Coastal and Ocean Engineering-Asce 125:98-108.